Chapter 5

MIMO-configured WLAN Access Point Antenna with High Port Isolation

5.1 Introduction

Multiple-input multiple-output (MIMO) configured internal antennas are in high demand for access point applications due to its advantage of high channel capacity without any additional cost of transmitted power and bandwidth [Winters (1987)]. The channel capacity increases linearly with the number of antenna elements in the MIMO system. However, the high packing density of the wireless devices causes strong mutual coupling between antenna elements. The mutual coupling hampers the MIMO antenna performance and deteriorates the channel capacity by providing correlated signals [Ni *et al.* (2012)]. The mutual coupling is mainly due to the space wave effect (near-field and far-field) and propagation of surface waves in the substrate of the printed antennas. The shorted antennas are the obvious choice for compact internal antennas. However, these antennas are strongly coupled due to the current in the common ground plane in an array architecture. The 15 dB isolation between antenna elements is considered sufficient for better signal reception. However, it is always advisable to obtain maximum possible isolation in the operating frequency band to avoid detrimental effects of practical device environment on antenna isolation characteristics [Meshram *et al.* (2012)].

A number of n-port ($n > 2$) MIMO antenna systems have been proposed in the last decade, but these are not able to achieve compactness and high isolation simultaneously [Guterman *et al.* (2006), Chiu and Murch (2008), and Karimian *et al.* (2012)]. Many isolation enhancement techniques have been proposed in the literature for various communication frequency bands to decouple antenna elements in n-port MIMO antenna

systems. In [Li *et al.* (2009)], a series of slits are arranged on the ground plane of a four-element MIMO antenna system to improve the isolation. These slits act as a band-stop filter and trap the coupling current. This method is useful to decouple the antennas when the strong current flowing through the ground plane. The work in [Choi and Lim (2015)] also utilized decoupling slits in the ground plane to enhance the isolation in electro-textile antenna based 4 x 4 MIMO array for mobile router applications. Such a pattern of slits, however, reduces the bandwidth. Antenna diversity technique was utilized in a four-element MIMO antenna for wireless local area network (WLAN) access point reported in [Liao *et al.* (2015)], and the coupling of −13 dB and −16 dB was obtained in 2.4 GHz and 5 GHz bands, respectively. However, to prevent the deterioration of the obtained isolation in practical device assembly, a further improvement in antenna decoupling is needed. In [Khan *et al.* (2015)], better than 17 dB isolation was achieved between four monopole antennas of a MIMO antenna array in the ultra wideband of 2.5–12 GHz utilizing polarization diversity. In [Sarkar *et al.* (2015)], better than 20 dB isolation was achieved in the quad bands with center frequencies of 1.95 GHz, 2.39 GHz, 2.64 GHz and 3.27 GHz between four element MIMO antenna array with the co-planar waveguide (CPW) fed monopole antennas utilizing polarization diversity. Recently, in [Malviya *et al.* (2017)], polarization diversity was utilized to decouple four patch antenna elements by better than −13 dB in the wideband of 1.68–2.24 GHz. However, in above three reported works, the separate ground plane is utilized by the antenna elements. Therefore, these antenna elements are not affected by the flow of current in the common ground plane. MIMO/diversity antenna systems for WLAN access point applications (2.4/5.2/5.8 GHz bands) employing polarization and spatial diversity to decouple the antenna elements was also proposed in [Su (2009), Su (2010), Su and Lee (2011), and Pan *et al.* (2016)]. However,

the proposed antenna structures have a large footprint to be installed as an internal antenna in the access point devices. It is observed from the state-of-the-art review presented above that the isolator based on the metamaterial structures in *n*-port ($n > 2$) MIMO systems are not addressed well. However, these structures have the potential to improve the decoupling between the antenna elements as observed in the state-of-the-art review presented in chapter 1 (section 1.4).

In this chapter, a compact four-element planar inverted-F antenna (PIFA) based MIMO antenna array is presented for 5 GHz WLAN applications (band 1: 5.15–5.35 GHz, band 2: 5.725– 5.825 GHz). The antenna elements are mirrored at the corners of the common ground plane to achieve pattern diversity along with the spatial diversity. Sufficient isolation level is achieved due to spatial/pattern diversity. However, to integrate the MIMO antenna in the complex environment of practical devices, isolation needs to be improved further so that the detrimental effects of device assembly on antenna isolation performance can be minimized. Therefore, a metasurface based isolator is placed between the antenna elements to improve isolation between them in the desired frequency bands. Section 5.2 of this chapter presents the antenna array without any isolator between the antenna elements. The proposed isolator and its operation mechanism are described in section 5.3. Section 5.4 presents the MIMO antenna with isolator structure in between the antenna elements and analyses the improvement in the isolation characteristics. The effect of the presence of isolator on the antenna radiation characteristics and MIMO/diversity performance is also discussed in this section. The simulated results are experimentally verified in section 5.5. The efficacy of the proposed isolation technique over some other metamaterial based isolator structures reported in the literature is presented in section 5.6. Finally, section 5.7 concludes the present chapter.

5.2 MIMO Antenna Array without Isolator

Planar inverted-F antenna that invokes the quarter wavelength operation is utilized for 5 GHz WLAN band and is designed using Equation 5.1 [Garg *et al.* (2001)] for the center frequency (5.5 GHz) of the band.

$$f = \frac{c}{4(L+W)} \tag{5.1}$$

where L and W are the length and width of the patch, f is the resonating frequency and c is the velocity of light in free space.

The antenna elements and ground plane are etched over a 0.8 mm thick FR4 substrate ($\varepsilon_r = 4.4, tan\delta = 0.02$) with an air gap of 4.2 mm in between. The four antenna elements are mirrored and placed at each corner of the ground plane and are fed by a coaxial probe. The position of the coaxial probe is adjusted with respect to the position of shorting post to achieve better impedance matching. The schematic of the designed MIMO antenna array is presented in Figure 5.1. The proposed structure is optimized to achieve −10 dB impedance bandwidth in the desired frequency band using Ansys HFSS software. The optimized parameters of the structure are as, l_s = 52 mm, w_s = 42 mm, l_p = 12 mm, w_p = 5 mm, l_{sh} = 1 mm, t = 4.2 mm, x = 6 mm, y = 4 mm. This schematic is referred as configuration 1 in rest of the chapter.

Figure 5.2 shows the *S*-parameter of the proposed MIMO antenna array. Due to the symmetry in the structure, $S_{11} = S_{22} = S_{33} = S_{44}$, $S_{21} = S_{34}$, $S_{31} = S_{24}$, $S_{41} = S_{32}$, and hence only S_{11}, S_{21}, S_{31} and S_{41} are plotted in the figure. It can be observed from the figure that the −10 dB impedance bandwidth of the proposed MIMO antenna is 1.395 GHz (4.825–6.22 GHz) covering the desired band 1 and band 2. Peak resonance is obtained at 5.38 GHz with the reflection coefficient of −16.42 dB. The shift in the resonance peak from the desired 5.5 GHz is due to the inductive effect of the coaxial probe which is not

included in the calculated value. Due to the presence of spatial and pattern diversity, the isolation varies in the range of 14.41–14.84 dB, 25.03–25.33 dB, 18.09–18.45 dB in band 1, and 15.93–16.28 dB, 26.80–27.39 dB, 19.25–19.54 dB in band 2 between antenna 1 and 2, antenna 1 and 3, and antenna 1 and 4, respectively. However, the isolation tends to deteriorate as the antenna array is integrated into the practical device environment, and hence further improvement in isolation is needed.

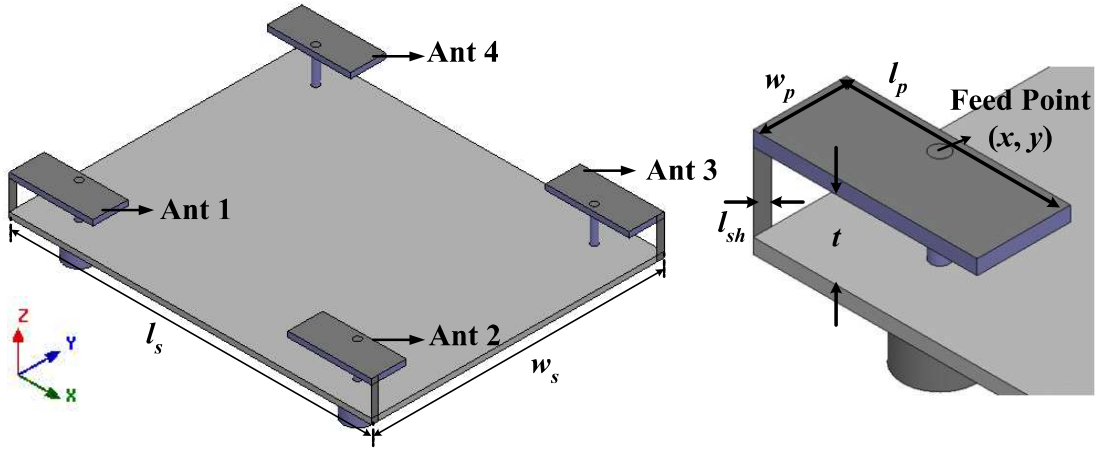

(a) (b)

Figure 5.1: (a) Schematic of the proposed MIMO antenna array, (b) enlarged view of single antenna element.

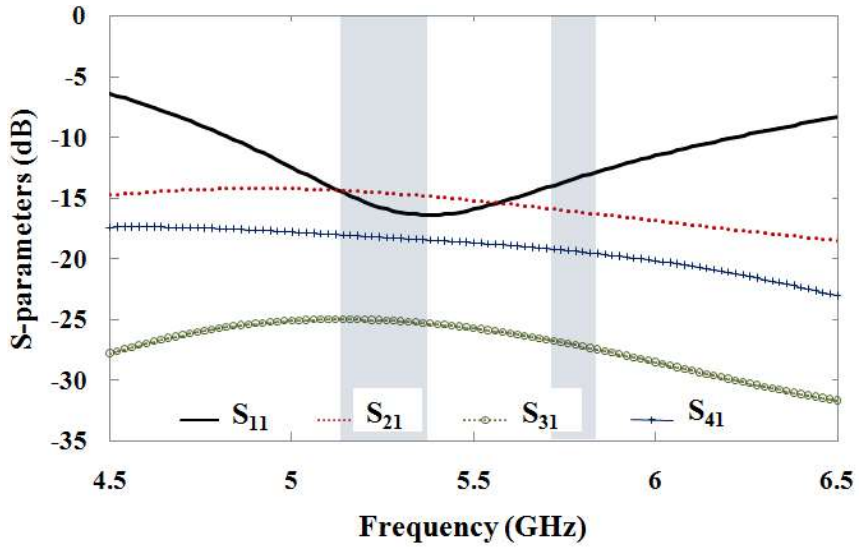

Figure 5.2: *S*-parameters of the proposed MIMO antenna array.

5.3 Design and Analysis of the Isolator

The main cause of coupling between the antenna elements presented in Figure 5.1 is observed as:

i. The radiated field of driven antenna element induces the voltage (called electromotive force) in the nearby placed antenna elements and causes the flow of current in them.

ii. The current through the common ground plane excites other antenna elements.

Considering the coordinate system shown in Figure 5.1, exciting element 1 only and keeping all other elements matched terminated, the maximum contribution in mutual coupling due to the radiated fields between element 1 and 2 is due to the field components appearing parallel to the plane of incidence (i.e. XZ plane). Similarly, the coupling due to the radiated fields between antenna element 1 and 4 is due to the field components parallel to its plane of incidence (i.e. YZ plane). Thus, parallel field components (also called TM polarized components) and not the perpendicular field components (also called TE polarized components) are identified as the cause of coupling. Therefore, the antenna elements could be decoupled if these TM polarized fields are reduced or eliminated by some decoupling structure. The propagation of the coupling current in the ground plane also need to be trapped to decouple the antenna elements properly.

To implement the above idea of decoupling the antenna elements, a structure is needed that could either absorb the TM polarized incident wave or cross-convert it into the TE polarized wave. As TE polarized wave is not observed as the cause of coupling in the proposed antenna configuration, therefore, for the TE polarized wave, the structure should behave as a co-polarized reflector only. The absorptivity of the structure for TE polarized wave should ideally be zero to prevent the deterioration of the

radiation efficiency of the antenna elements. Such a behavior can be obtained from the metasurfaces because the electromagnetic response of these structures can be adjusted as per the requirement by varying the resonator geometry. As observed in previous chapters that the metasurface structure with symmetricity in the two orthogonal directions provides an identical response for the TE and TM polarized incident waves. Therefore, the asymmetrical unit cell would be more useful here as a different response is required for the TE and TM polarized wave.

The metasurface employed in this chapter (shown in Figure 5.3) is a variant of the unit cell structure presented in chapter 2. To attain asymmetric unit cell, square geometry is converted into the rectangular one. It is observed through simulation that on reducing the cell dimension along the direction of TE polarized wave, the absorptivity of the structure is high with a certain amount of cross-polar reflected power for TM polarized normally incident wave. While for TE polarized normally incident wave, the absorptivity of the structure reduces drastically and most of the power gets reflected in co-polarization itself. The number of diagonal arms in the proposed unit cell also reduced to one instead of four presented in the previous unit cell to make the geometry anisotropic. The anisotropy of the unit cell structures contributes to the generation of cross-polar reflection from the structure [Lin *et al.* (2016)]. The higher cross-polar reflection for the fixed value of co-polar reflection reduces the absorptivity of the structure, and hence the antenna radiation efficiency does not deteriorate much. The boundary conditions, port excitation and substrate parameters of the proposed metasurface unit cell are same as that reported in previous chapters. The simulations are performed using CST microwave studio. The unit cell is optimized to obtain desired reflection/absorption response in the 5 GHz WLAN band. The optimized geometrical

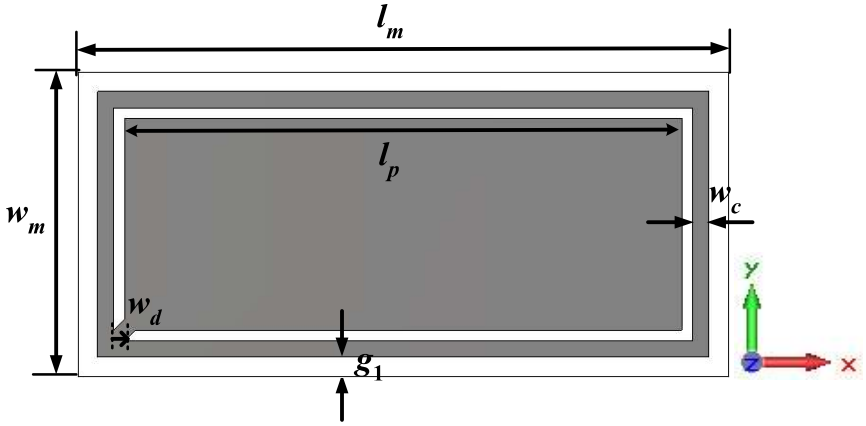

Figure 5.3: Design of the proposed metasurface unit cell.

parameters are, l_m = 12 mm, w_m = 5.65 mm, l_p = 10.28 mm, g_1 = 0.36 mm, w_c = 0.3 mm, w_d = 0.2 mm.

The reflection and absorption characteristics of the proposed metasurface are presented for TM and TE polarized normally incident wave in Figure 5.4(a) and (b), respectively. The transmittivity of the structure is zero due to the complete metallic backplane. The absorption of the structure is calculated using Equation 5.2.

$$A(\omega) = 1 - R(\omega) \tag{5.2}$$

where, $R(\omega) = \left|S_{11,co}\right|^2 + \left|S_{11,cross}\right|^2$. $S_{11,co}$ and $S_{11,cross}$ are the co- and cross-polar reflection coefficients as defined by Equation 5.3 and 5.4, respectively.

$$S_{11,co} = \frac{|E_{mr}|}{|E_{mi}|} \tag{5.3}$$

$$S_{11,cross} = \frac{|E_{nr}|}{|E_{mi}|} \tag{5.4}$$

where m and n are x and y, respectively for TM polarized wave. For TE polarized wave, m and n are y and x, respectively. The subscript i and r indicate the incident and

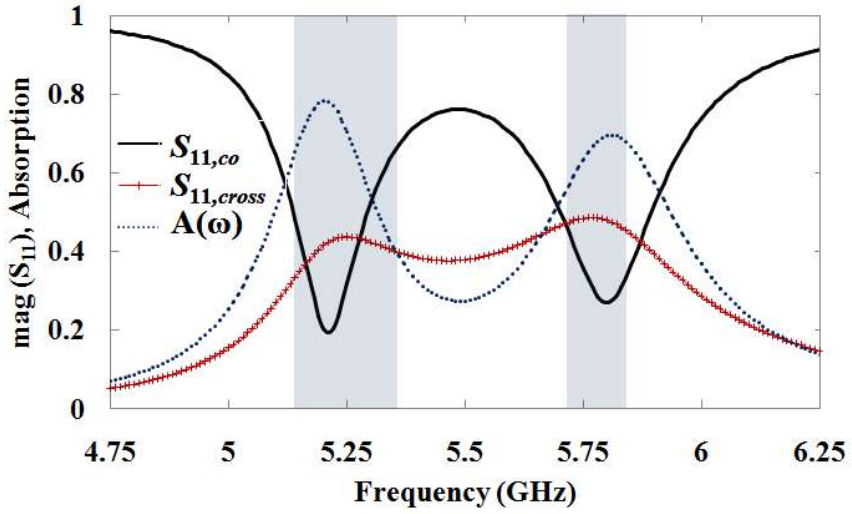

(a)

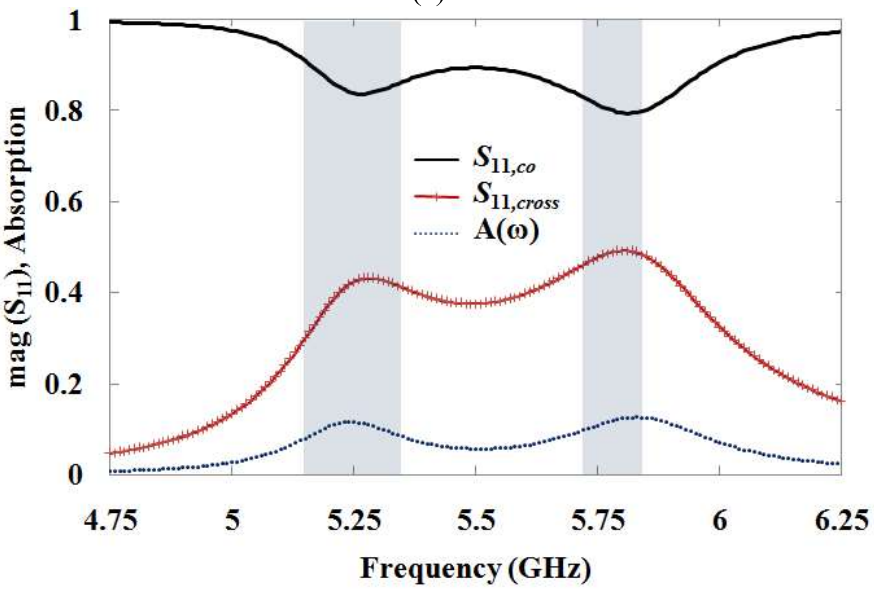

(b)

Figure 5.4: Reflection and absorption characteristics of the proposed metasurface for normally incident (a) TM polarized wave and (b) TE polarized wave.

reflected signals, respectively. It is observed from Figure 5.4(a) that the minimum co-polar reflected power ($=\left|S_{11,co}\right|^2$) is obtained as 3.74% and 7.33% at 5.21 GHz and 5.8 GHz, respectively for parallel polarized wave (TM). The absorptivity of the structure is 78.24% and 69.6%, and cross-polar reflected power ($=\left|S_{11,cross}\right|^2$) is 18.02% and 23.07% at 5.21 GHz and 5.8 GHz, respectively. Hence, it can be concluded that the proposed

metasurface is absorbing the major portion of the incident power and reflects the rest of the power with orthogonal polarization. Figure 5.4(b) depicts that for the TE polarized case, the co-polar reflected power become high (73.85% and 63.34% at 5.21 GHz and 5.8 GHz, respectively) while cross-polar reflected power remains almost the same (15.10% and 24.30% at 5.21 GHz and 5.8 GHz, respectively), which in turn significantly reduces the absorptivity (11.05% and 12.37% at 5.21 GHz and 5.8 GHz, respectively) of the structure in the desired bands.

The incident wave may fall on the structure at any angle of incidence 'θ', and hence co-polar and cross-polar reflection coefficients of the proposed structure are presented under the obliquely incident TM and TE polarized wave in Figure 5.5(a) and (b), respectively. It is observed that resonance shifts towards higher frequency side with an increase in angle of incidence. It is due to the decrease in the induced fields on the structure that ultimately shorten the current path length with increasing angle 'θ'. The structure is working well in the desired band up to an angle of incidence of 30^0.

5.4 MIMO Antenna Array with Enhanced Isolation

A 1 x 2 array of a unit cell of the metasurface based isolator presented in the previous section is placed in between each pair of PIFA elements to increase the isolation as shown in Figure 5.6. The presented antenna configuration is referred as configuration 2 in rest of the chapter. The placement of the isolator in the proximity of PIFA elements led to the strong electromagnetic coupling. Therefore, the proposed MIMO antenna elements and isolator structure is further optimized using Ansys HFSS software. The modified set of dimensions is: l_s = 52, w_s = 42, l_p = 12, w_p = 7, l_{sh} = 1, t = 4.2, x = 6, y = 6, l_m = 13.65, w_m = 6, l_p = 11.45, G_2 = 0.4, w_c = 0.4, w_d = 0.2 (all dimensions are in mm).

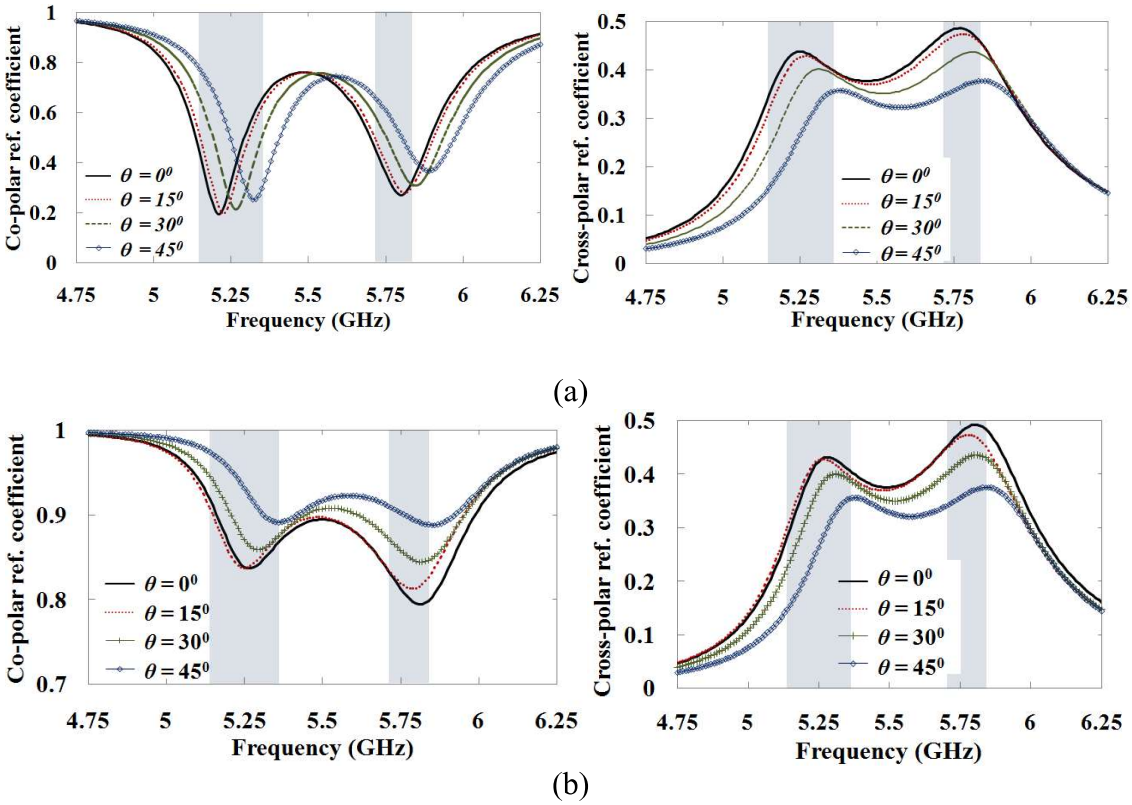

Figure 5.5: Co-polar and cross-polar reflection coefficient under the variation of the angle of incidence for (a) TM polarized and (b) TE polarized incident wave.

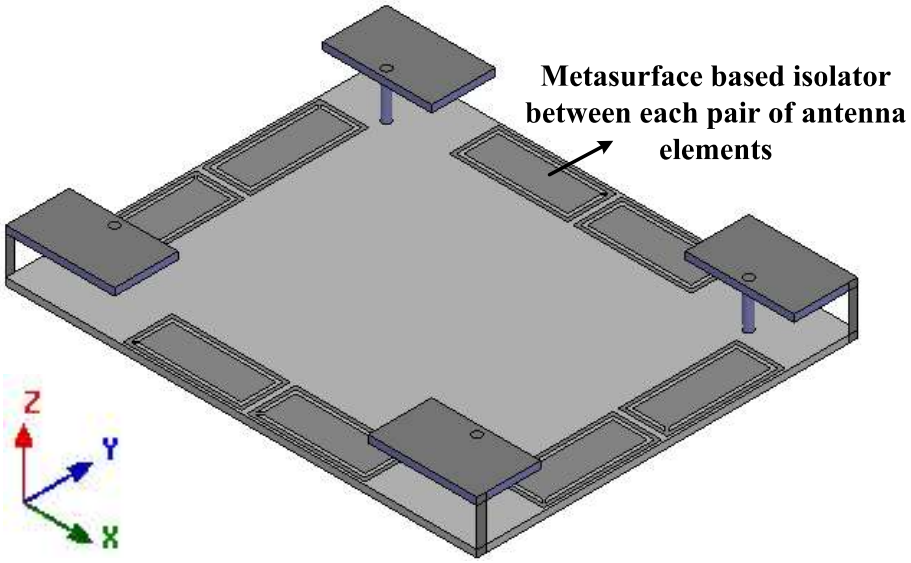

Figure 5.6: Proposed MIMO antenna array with isolator.

The reflection coefficient characteristics (S_{11}, S_{22}, S_{33}, S_{44}) of the proposed antenna configuration 2 is presented in Figure 5.7(a). It is observed that the reflection coefficients are below −10 dB level in the desired bands covering a bandwidth of 1.5 GHz (4.45–5.95 GHz), which shows proper impedance matching of the antenna elements with the feeding probe. The transmission coefficient characteristics of the antenna configuration 1 and 2 are compared in Figure 5.7(b), (c), and (d). Only S_{21}, S_{31}, S_{41} are presented as $S_{21} = S_{34}$, $S_{31} = S_{24}$, $S_{41} = S_{32}$ due to symmetry in the structure. It is observed that the transmission coefficients decreases sharply in the desired bands and hence isolation increases in the presence of isolator. The maximum obtained isolation in band 1 and band 2 with and without the presence of isolator are summarized in Table 5.1. The values clearly indicate the effectiveness of the proposed isolator in MIMO antenna array.

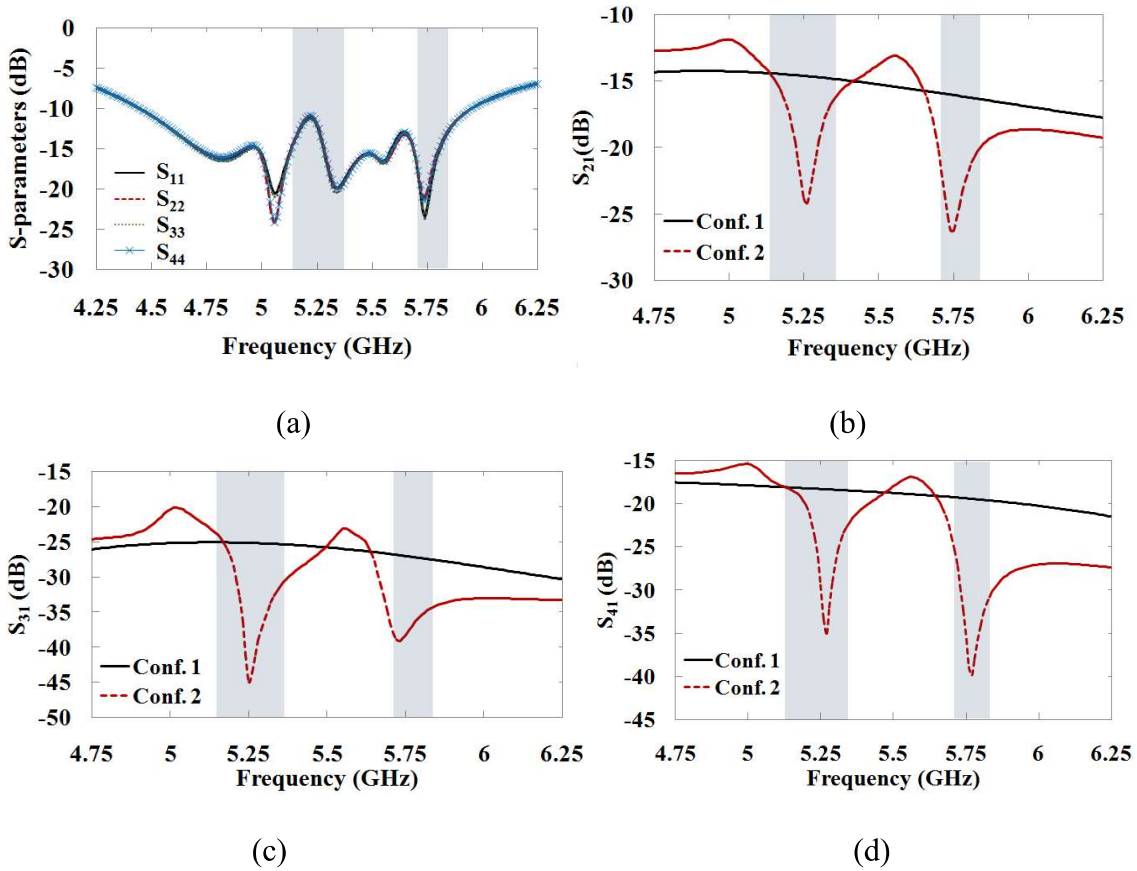

Figure 5.7: (a) Simulated reflection coefficients of the proposed antenna conf. 2, comparison of transmission coefficients of the conf. 1 and 2 (b) S_{21}, (c) S_{31}, and (d) S_{41}.

Table 5.1: Maximum Observed Isolation between Various Antenna Pairs of the Proposed MIMO Antenna Array

Antenna Pair	Band 1			Band 2		
	Conf. 1	Conf. 2	Improvement	Conf. 1	Conf. 2	Improvement
Ant. 1 & 2	14.82 dB	24.17 dB	9.35 dB	16.31 dB	26.23 dB	9.92 dB
Ant. 1 & 3	25.30 dB	44.92 dB	19.62 dB	27.45 dB	39.04 dB	11.59 dB
Ant. 1 & 4	18.43 dB	34.98 dB	16.55 dB	19.57 dB	39.80 dB	20.23 dB

5.4.1 Surface Current Density

To better understand the operation mechanism of the used isolator, plot of surface current density is presented for 5.25 GHz and 5.78 GHz in Figure 5.8(a) and (b), respectively. These plots are shown by keeping antenna 1 excited and all other antennas matched terminated with 50 Ω impedance (characteristics impedance of the feed line). It is observed that in the antenna configuration 1, significant current couples to other antenna elements when one antenna is excited. In the presence of the proposed isolator between the antenna pairs, the coupling current flowing through the ground in port 2, 3 and 4 is observed as antiparallel to the current in the resonator of the metasurface array, and hence magnetic resonance generates in the metasurface. This magnetic resonance is responsible for the desired reflection/absorption characteristics in the frequency bands of interest and also traps the flow of current through the common ground plane. Therefore, the coupling between the antenna ports is greatly reduced and high isolation is achieved.

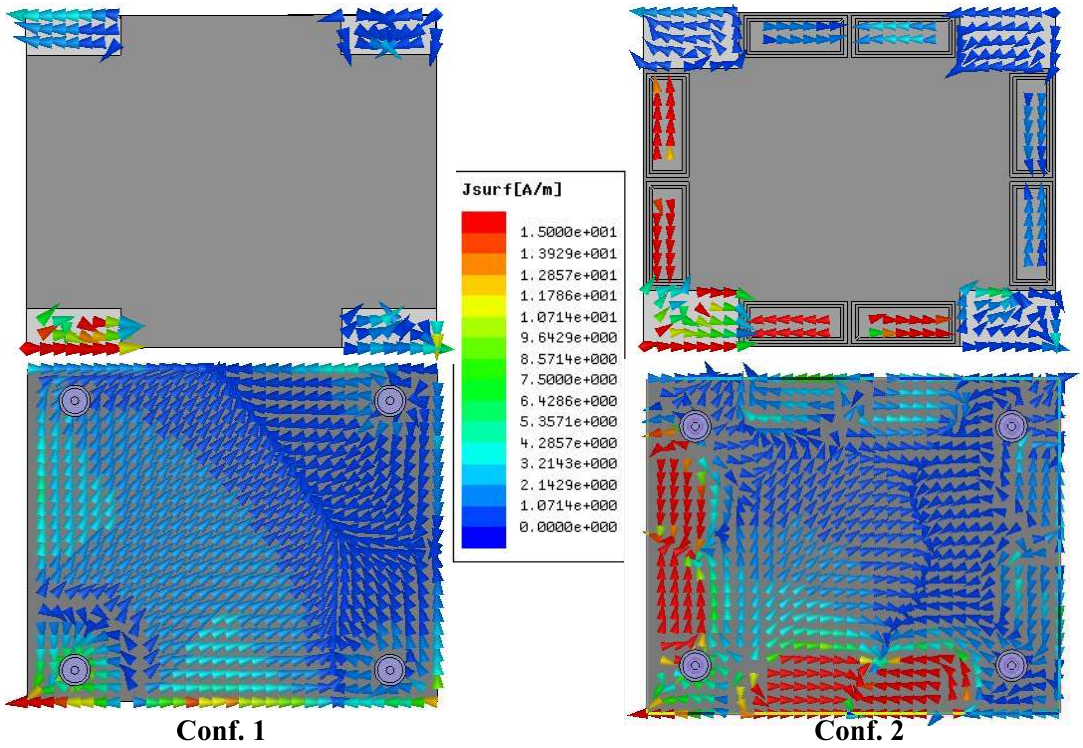

(a)

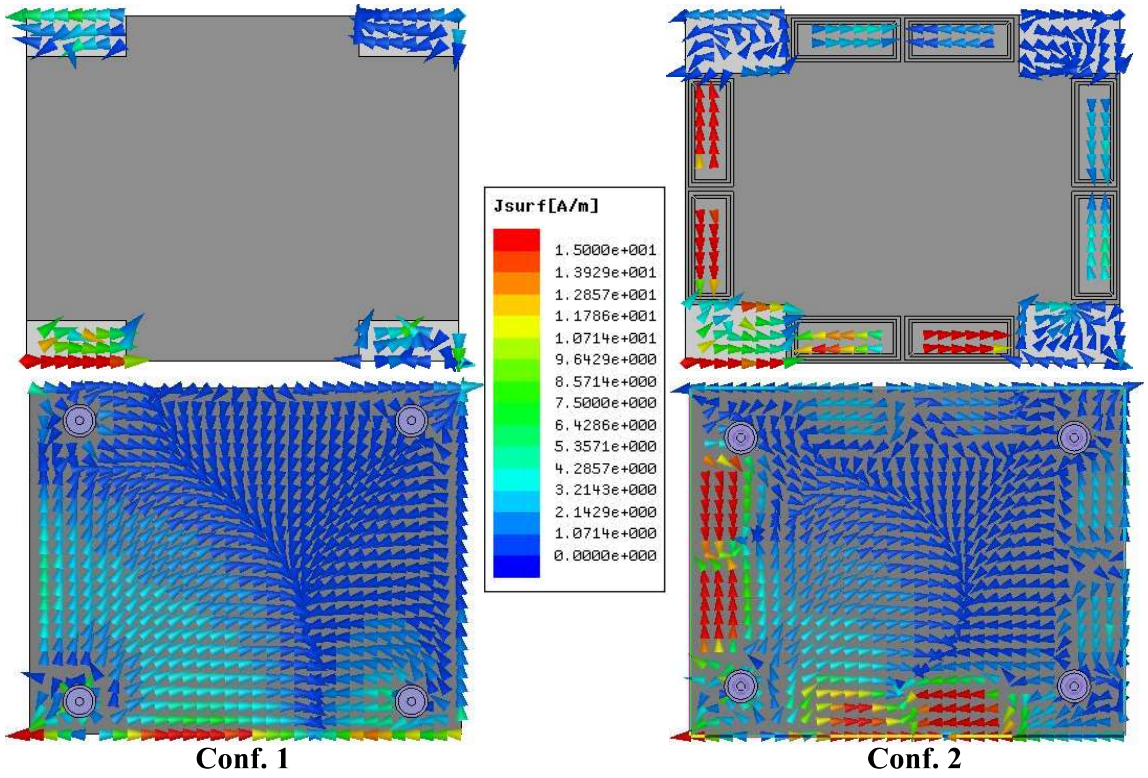

(b)

Figure 5.8: Surface current distribution in the proposed antenna system by keeping antenna 1 excited and all other antennas matched terminated at (a) 5.25 GHz, and (b) 5.78 GHz.

5.4.2 Radiation Characteristics

The simulated radiation patterns of the proposed antenna configuration 1 and 2 at 5.25 GHz are shown in Figure 5.9 by exciting one antenna at a time and keeping all other antennas matched terminated. Radiation patterns at all other frequencies of interest are having almost similar behavior as evident from the surface current plots presented in Figure 5.8 and hence, are not presented. It can be clearly observed from the figure that the radiation patterns of the antenna pairs 1-2 and 3-4 are having pattern diversity in XZ and XY planes, while antenna pairs 1-4 and 2-3 are having pattern diversity in YZ and XY planes. Therefore, in the deep fading environment, at least one of the antenna elements pick up the desired signal.

The radiation efficiency and peak realized gain of the antenna array conf. 1 and 2 by keeping antenna 1 excited and all other antenna elements matched terminated is presented in Figure 5.10(a) and (b), respectively. It is observed from the figures that the radiation efficiency and hence, the peak realized gain of the antenna element decreases in the presence of isolator. This is because of the absorption of the significant portion of the radiated field in the isolator structure itself. However, for array configuration 2, the radiation efficiency varies from 58.45–84.28 % and 63.80–87.71 % and the peak realized gain varies between 0.49–3.50 dBi and 1.32–3.40 dBi for band 1 and band 2, respectively. These values are sufficient to use the proposed structure for indoor applications.

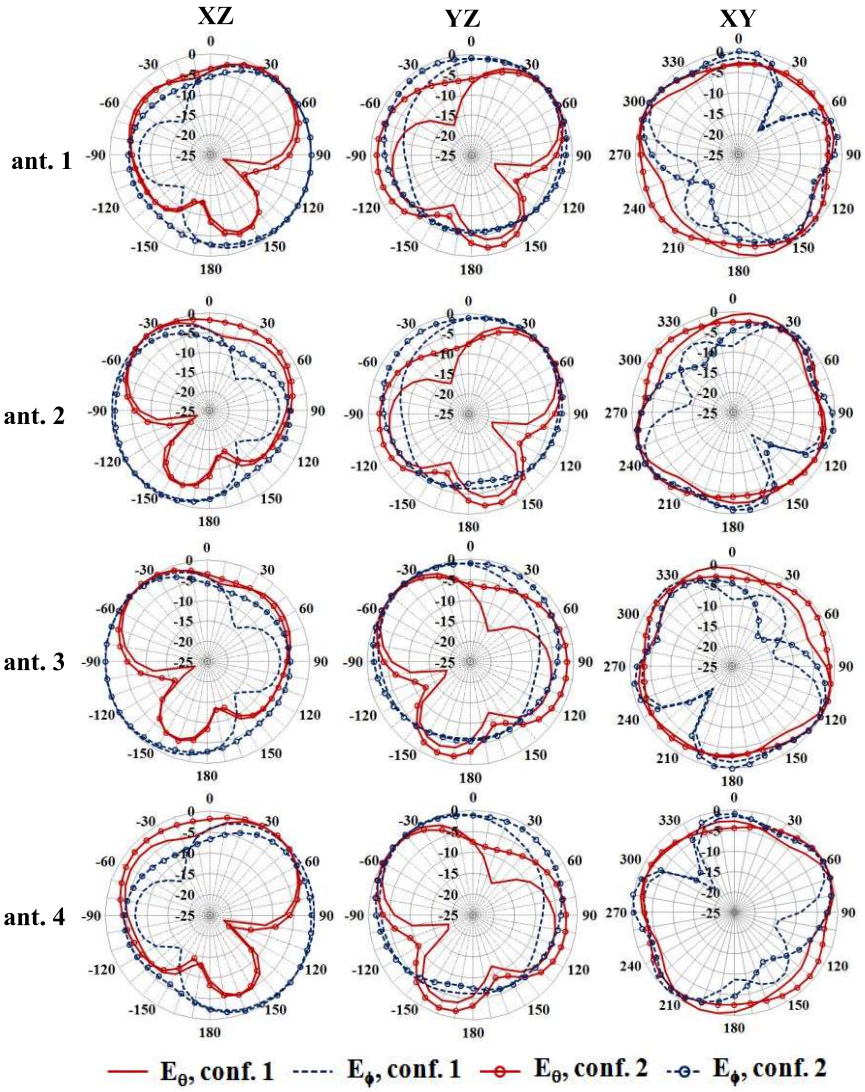

Figure 5.9: Radiation patterns of the proposed MIMO antenna array at 5.25 GHz for one antenna excited at a time keeping all other matched terminated.

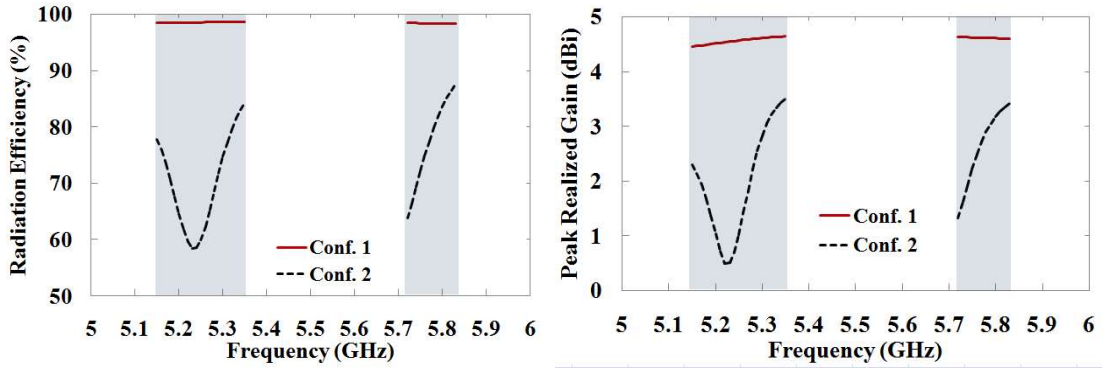

(a) (b)

Figure 5.10: (a) Radiation efficiency and (b) peak realized gain of the array configuration 1 and 2 for antenna 1 excited and all other antenna elements matched terminated.

5.4.3 MIMO Characteristics

To account for the antenna correlation in the proposed four-element MIMO antenna system (conf. 1 and 2), envelope correlation coefficient (ECC, ρ_e) between various antenna pairs is calculated using Equation 5.5 [Thaysen and Jakobsen (2006)] and is shown in Figure 5.11.

$$\rho_e(i,j) = \frac{\left| \sum_{n=1}^{N} S_{i,n}^{*} S_{n,j} \right|^2}{(1 - \sum_{n=1}^{N} S_{i,n}^{*} S_{n,i})(1 - \sum_{n=1}^{N} S_{j,n}^{*} S_{n,j})} \tag{5.5}$$

where, N is the total number of ports in the MIMO antenna system, and i and j are the number of antenna elements. The calculated ECC values in the desired bands are well below the standard limits (<0.5) set for wireless communication devices for both the array configurations. Thus, the proposed antenna arrays are suitable to be used for MIMO application. It is further observed that the configuration 2 has much lesser ECC values (tending towards zero) in the desired bands compared to that of configuration 1. Hence, the proposed isolator is lowering the antenna correlation significantly in the desired bands.

Diversity gain is an important figure of merit for the characterization of diversity antenna systems. The apparent diversity gain (G_{app}) is obtained by multiplying the maximum apparent diversity gain by the correlation efficiency (e_p) [Schwartz *et al.* (1965), p. 474]. The value of the maximum apparent diversity gain is 10 dB considering 1% cumulative density function (CDF) using selection combining. The correlation efficiency is related to the ECC as given in Equation 5.6. The apparent diversity gain value indicates that how much the maximum apparent diversity gain reduces in the presence of correlation between antenna elements. Likewise, the effective diversity gain (EDG) can be calculated by multiplying the apparent diversity gain by the antenna radiation efficiency [Kildal *et al.* (2002)]. The calculated values of apparent diversity

gain between all three antenna pairs for the proposed antenna arrays (conf. 1 and 2) are presented in Figure 5.12. It is observed that the G_{app} is much closer to the maximum value of 10 dB in the desired bands for antenna configuration 2 as compared to the configuration 1 which represent that the antenna elements in configuration 2 are strongly decoupled, and hence justifies the efficacy of the proposed isolator. It is already observed that the radiation efficiency of the antenna elements reduces in the presence of the proposed isolator, hence, the EDG values for configuration 2 are less compared to configuration 1. The obtained EDG values between various antenna pairs for configuration 1 are 9.937 dB and 9.929 dB at 5.25 GHz and 5.78 GHz, respectively. The corresponding values for configuration 2 are 7.779 dB and 9.021 dB at 5.25 GHz and 5.78 GHz, respectively. These values are obtained by taking antenna 1 as the reference branch. The EDG values for all three antenna pairs are found very close to each other in the desired bands because of the very small variation (9.9999 dB to 10 dB only) of the apparent diversity gain.

$$e_p = \sqrt{1-|\rho_e|^2} \tag{5.6}$$

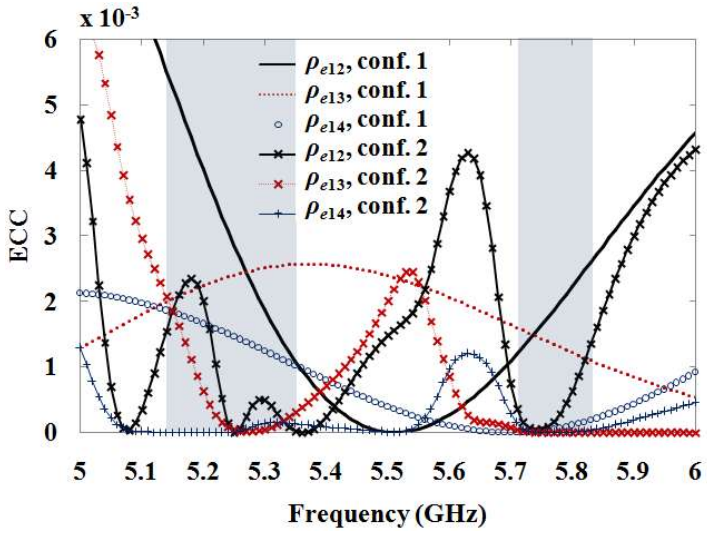

Figure 5.11: Envelope correlation coefficient between various antenna pairs for the proposed MIMO antenna array.

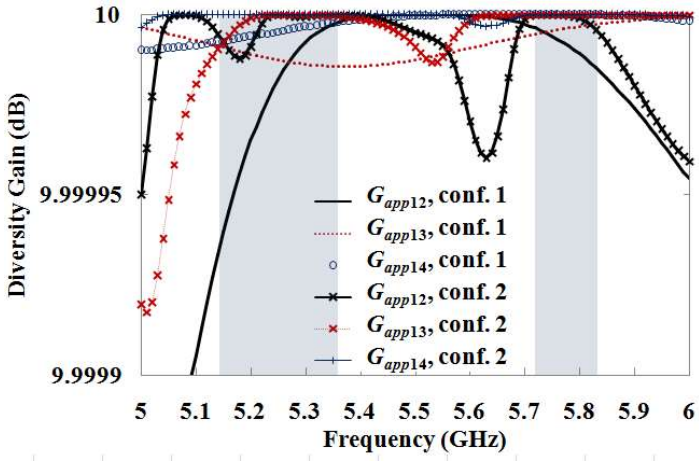

Figure 5.12: Diversity gain between various antenna pairs of the proposed MIMO antenna array.

5.5 Experimental Verification

A prototype of the proposed four-element MIMO antenna is fabricated and is shown in Figure 5.13. *S*-parameters of the proposed MIMO antenna is measured using Anritsu VNA (vector network analyzer) Master MS2038C and are presented in Figure 5.14(a)–(d). In Figure 5.14(a), the measured reflection coefficients are compared with simulated S_{11} only due to the almost similar simulated reflection response for all four antenna elements (see Figure 5.7(a)). The measured results show that the −10 dB impedance bandwidth of the proposed MIMO antenna is 1.54 GHz (4.32–5.86 GHz), and is covering the desired frequency bands (band 1: 5.15–5.35 GHz, band 2: 5.725–5.825 GHz). Peak measured isolation (see Figure 5.14(b)–(d)) of 26.7 dB, 41.3 dB, and 46.1 dB is obtained in band 1, and 28.5 dB, 34.9 dB, and 39.0 dB is obtained in band 2 between antenna pairs 1-2, 1-3, and 1-4, respectively. The measured results are found in good agreement with the simulated results. The measured and simulated radiation patterns of the proposed MIMO antenna array (conf. 2) in three principal planes for vertical (E_θ) and horizontal (E_ϕ) polarization at 5.25 GHz are presented in Figure 5.15. The radiation patterns are plotted by keeping antenna 1 excited and all other antenna

elements matched terminated. The measured radiation patterns are in close agreement with the simulated radiation patterns. The radiation pattern is quasi omnidirectional in nature, and hence suitable for indoor wireless applications.

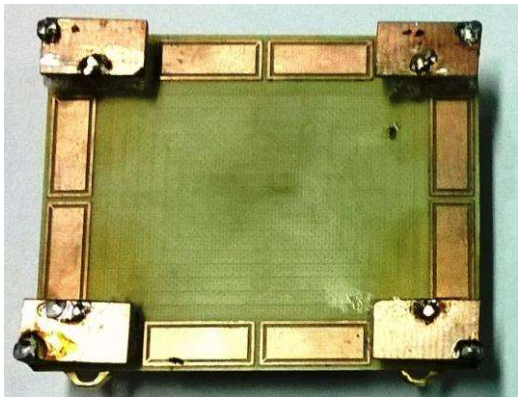

Figure 5.13: Fabricated prototype of the proposed MIMO antenna.

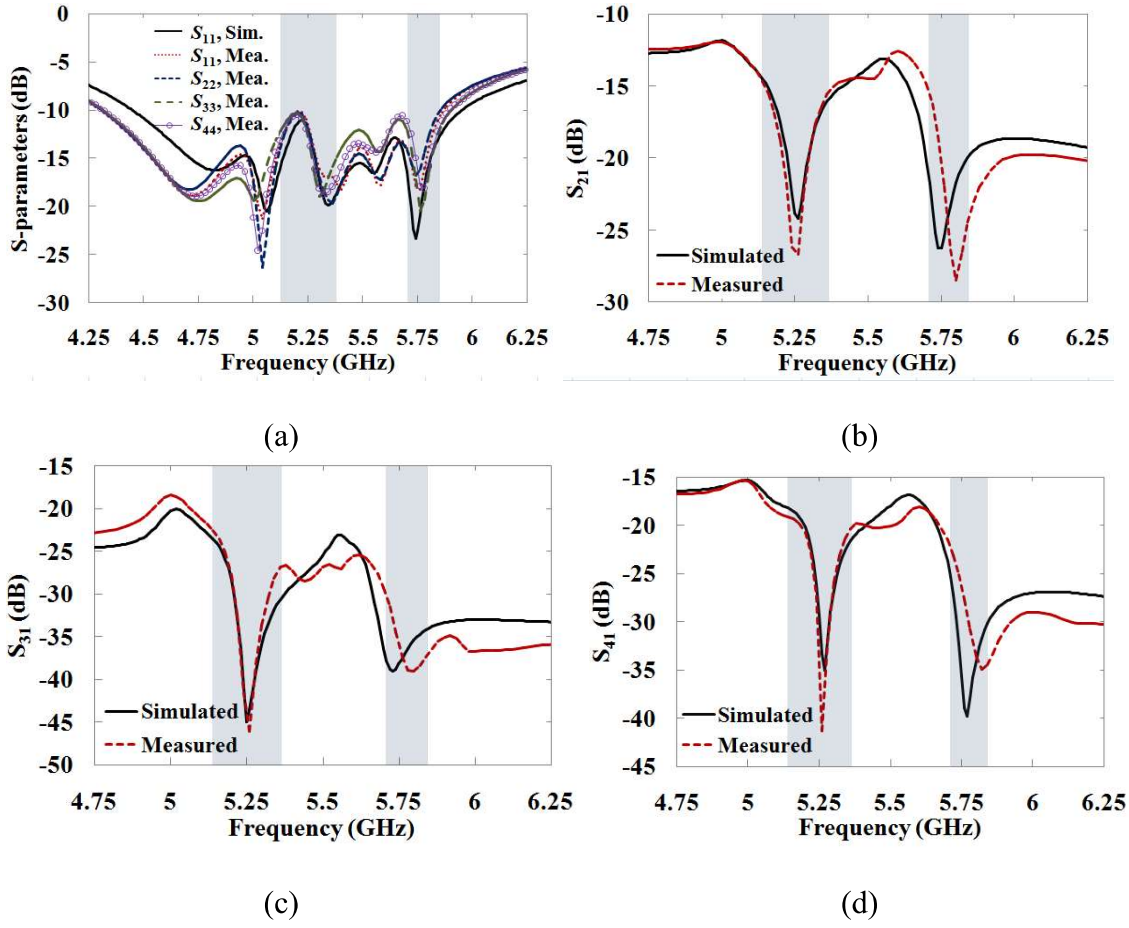

Figure 5.14: (a) Reflection and transmission coefficient characteristics (b) S_{21}, (c) S_{31}, (d) S_{41} of the proposed MIMO antenna.

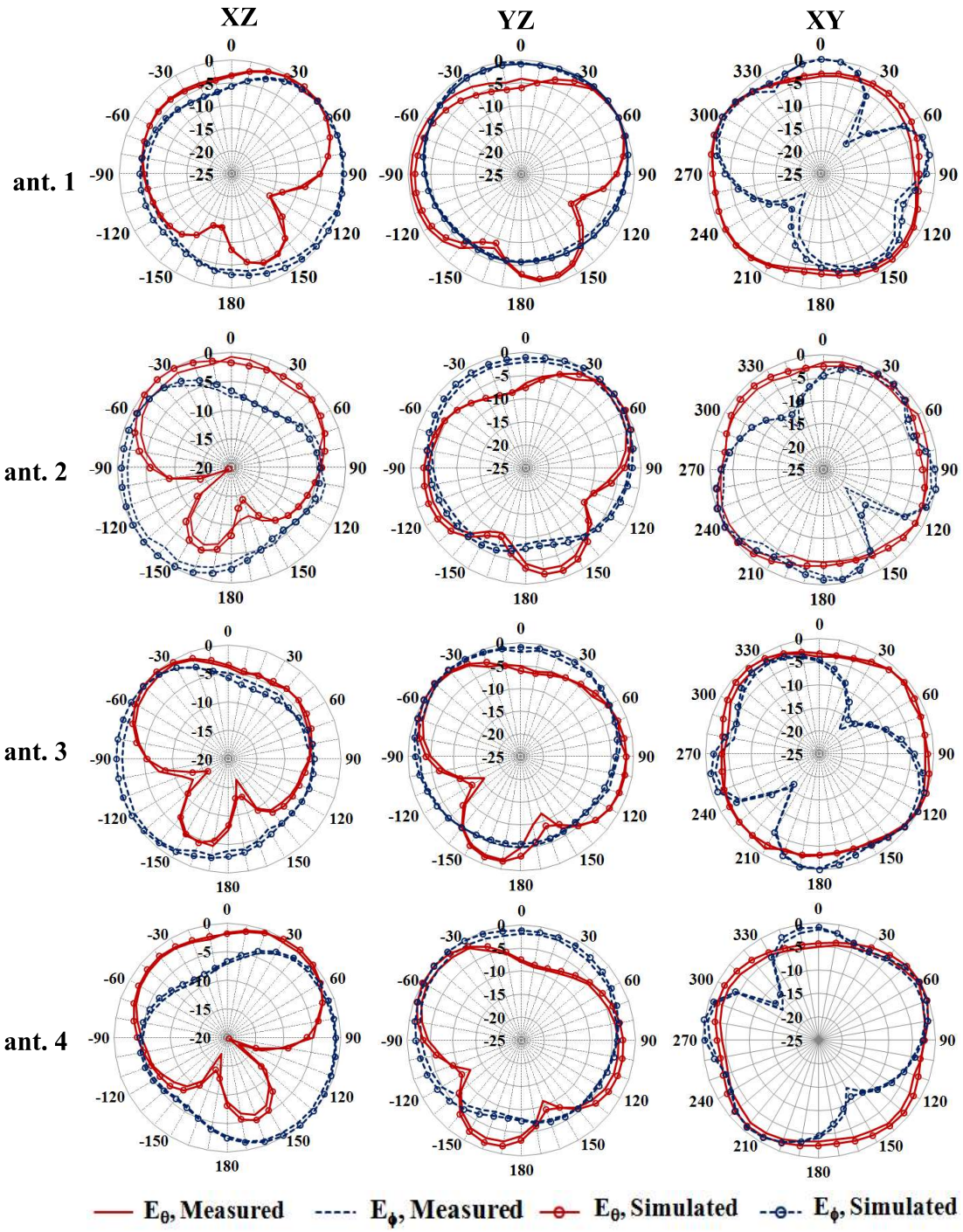

Figure 5.15: Measured radiation pattern of the proposed MIMO antenna array (conf. 2) by exciting one antenna element and keeping all other matched terminated.

5.6 Performance Comparison of the Proposed Isolator with Other Metamaterial Based Isolators

The isolation enhancement performance of the proposed isolator is compared with some other metamaterial/metasurface based isolator structures reported in the literature in Table 5.2. It is observed that the proposed isolation enhancement technique is a promising technique to decouple closely spaced antenna elements in multi-element antenna systems.

Table 5.2: Performance Comparison of the Proposed Isolator

Reference	Isolation Technique	No. of Ant. Elements	Frequency Band	Antenna Spacing	Isolation Improvement
[Yang and Samii (2003)]	Mushroom type EBG	2	5.8 GHz	$0.75\lambda_{5.8\ GHz}$	8 dB
[Bait-Suwailam *et al.* (2010)]	CSRRs	2	5 GHz	$0.25\lambda_0$	10 dB
[Tang *et al.* (2010)]	SRR and CSRR	2	5.82 GHz	$0.5\ \lambda_0$	9.07 dB
[Lee and Lee (2011)]	Metamaterial absorber	2	2.45 GHz	$0.23\lambda_{2.45\ GHz}$	11.2 dB
[Yoon *et al.* (2012)]	Metamaterial absorber	2	1.92-2.17 GHz	20 mm	~ 10 dB
[Wei *et al.* (2014)]	Metamaterial absorber wall	2	1.65-3.3 GHz	Center spacing of 110 mm	10 dB
[Khan *et al.* (2014)]	SRR	4	2.45 GHz	$0.1\lambda_{2.45\ GHz}$	7 dB
[Ramachandran *et al.* (2016)]	CSRR	Collocated MIMO (4 ports)	2.4 GHz ISM band	--	6.5 dB
[Hafezifard *et al.* (2016)]	Metamaterial substrate	2	5.1-5.9 GHz	$0.073\lambda_0$	12–19 dB
Proposed	Asymmetrical metasurface	4	2 (5.15-5.35 GHz and 5.725-5.825 GHz)	$\sim 0.5\lambda_{5.5GHz}$	9.35 -20.23 dB between various antenna ports

5.7 Conclusion

A four-element MIMO antenna array suitable for 5 GHz WLAN access point applications has been presented in this chapter. Sufficient isolation between antenna elements was obtained utilizing spatial/pattern diversity. To prevent the deteriorating effect of the practical device assembly on the antenna isolation characteristics, a metasurface based isolator has been placed between the antenna elements. The reflection response of the proposed metasurface has been discussed in detail. The proposed isolator significantly improved the isolation between various antenna pairs. The capability of the proposed isolator to decouple the antenna elements has been explained with the help of surface current distribution plot. The effect of the isolator on the radiation patterns, radiation efficiency, and peak realized gain has been discussed, and it was found that all values are suitable to use the proposed antenna array for indoor applications. ECC values for all three antenna pairs were well below the standard limit set for wireless communication devices and thus, the proposed antenna array found suitable for MIMO application. The diversity capability of the proposed antenna array has been evaluated in terms of apparent and effective diversity gain. The simulated results of the proposed MIMO antenna array have been validated with the experimental results and found in close agreement.

A summary and conclusion of the presented work so far in this thesis are provided along with the key findings in the next chapter. A scope for the further work on the related topics is also listed.

Left Intentionally